UNIVERSITY OF OKLAHOMA

GRADUATE COLLEGE

ENHANCED ASSESSMENTS OF TORNADO LOCATIONS AND DAMAGE USING GEOSPATIAL TECHNOLOGIES

A THESIS

SUBMITTED TO THE GRADUATE FACULTY

in partial fulfillment of the requirements for the

Degree of

MASTER OF SCIENCE

By

ROBERT MOORE

Norman, Oklahoma

2024

ENHANCED ASSESSMENTS OF TORNADO LOCATIONS AND DAMAGE USING GEOSPATIAL TECHNOLOGIES

A THESIS APPROVED FOR THE

DEPARTMENT OF GEOGRAPHY AND ENVIRONMENTAL SUSTAINABILITY

BY THE COMMITTEE CONSISTING OF

Dr. Michael Wimberly, Chair

Dr. Kirsten de Beurs

Dr. Michael Biggerstaff

TABLE OF CONTENTS

ABSTRACT

Tornado climatologies represent an important tool for understanding the genesis, behavior, and dissipation of tornados and tornadic storms. The current tornado record is imperfect, but nevertheless useful. I undertook a study to construct a tornado climatology for the state of Alabama in order to test theories about the influence of surface heterogeneities on tornadogenesis as well as human-caused bias. Support was found for the notion that tornados may occur atop higher elevations more frequently in Alabama, but other orographic effects were more difficult to discern. The most strongly correlated variable tested was road proximity, suggesting that accessibility to surveyors has an outsized influence on where tornadogenesis points are recorded. In an effort to explore additional ways of detecting tornadic damage, a second study was undertaken to explore the utility of Sentinel-2 derived disturbance index imagery. The disturbance index was shown to be positively correlated with damage intensity across all land cover types. Actual values of disturbance index for a given damage intensity were highly variable, even within a land cover classification. The lower threshold of detectability was somewhere between higher end EF1 and lower end EF2 events. While this does not represent an improvement in detectability threshold over previous studies, the methodology presented, in conjunction with the use of Sentinel-2, has several advantages such as only requiring a single post-event image for analysis and increased spatial detail in the output compared to previous studies. The results were summarized across land cover type and damage intensity and predictive performance was much better in the types of forested areas for which the DI was designed. Although this is a limitation overall, the strengths of the methodology counterbalance the weaknesses of traditional ground-based survey methods.

Introduction

For well over one hundred years, tornado climatologies have formed an important part of the pursuit for understanding how tornados and tornadic storms form, behave, and dissipate (Finley 1884; Dixon et al. 2011). Studies have been undertaken using tornado climatologies in efforts to understand public risk perception (Johnson et al. 2021), forecast improvement and dynamical understanding (e.g., Kellner and Niyogi 2014; Hua and Chavas 2019), and for infrastructure and public safety planning (e.g., Ramsdell et al. 2007). Despite the importance of a robust understanding of tornado climatology, a variety of data quality issues have long been known and discussed in the literature (Doswell and Burgess 1988). Over time, definitions and thresholds have been updated (McDonald and Mehta 2006), and analysis techniques have been developed to mitigate some issues and draw more meaningful conclusions from these imperfect data (Brooks et al. 2003; Verbout et al. 2006), but the ongoing record continues to rely on ground based surveys conducted by in-situ personnel. This thesis identifies some of the inherent limitations of this method and the effects that it can have on the historical record as well as exploring a potential supplementary detection method using satellite remote sensing.

One of the many applications of tornado climatologies is planning in advance of major field campaigns that seek to observe tornados. Combining an understanding of tornado occurrence probabilities with the necessary conditions for the various instruments involved allows for a more thorough plan of operations and allows for more logistics to be worked out in advance. One such project, Propagation and Evolution of Rotation in Linear Storms (PERiLS), occurred in the late winter and early spring of 2022 and 2023. PERiLS involved the deployment of over 100 in-situ and ground based remote sensing instruments from over a dozen institutions to characterize the environment in and around tornadic, linear storms as the occurred in the

Southeastern United States and Mississippi Delta regions (NSSL). In 2019, I was asked to do a brief analysis of the tornado climatologies in potential operating areas for PERiLS to support planning and decision making.

From that tornado climatology analysis, I was given the additional task of assessing any patterns relating to surface heterogeneities and the locations of tornadic initiation. Recent literature has variously suggested that transitions in land cover type (Kellner and Niyogi 2014; Frazier et al. 2019), positively and negatively sloping terrain (Schneider 2009; Hua and Chavas 2019), higher elevation, and valley flows (Lyza and Knupp 2018) could all serve to enhance tornadogenesis potential. While assessing these hypotheses in the state of Alabama, I noticed that, visually, a far stronger correlation appeared to exist between tornadogenesis locations and roadways. Chapter one reports a study of elevation, surface roughness, and road proximity alongside population density, which is known to be a bias in the tornado record. Road proximity is shown to demonstrate the strongest relationship with tornadogenesis locations. This is explainable by the limitations of ground-based survey methods, especially in areas where access and visibility can be poor, such as in the varied terrains of rural Alabama.

Given the importance of a robust tornado climatology, it is clear that additional survey methods are desirable, both to reduce the burden of surveys on the operational NWS personnel that conduct them and to reduce the effects of biases inherent to ground survey methods. Previous work has demonstrated the utility of satellite remote sensing for this purpose (e.g., Molthan et al. 2014; Kingfield and de Beurs 2017). Landsat imagery has been able to detect the damage swaths from tornados down to lower end EF2 events using a tasseled cap-derived disturbance index. Since that study was conducted, tasseled cap indices have become available for the higher resolution imagery captured by Sentinel-2. In order to see if the improved

resolution could yield a lower damage threshold for detection, we selected fourteen scenes containing a total of fifty tornados and representing a broad cross-section of damage intensity, path width, landcover type, geographic region, and seasonality. The remote sensing techniques explored here are found to work best in forested areas and wetlands, which are typically the same kinds of low population density, low visibility, and low accessibility areas where traditional ground-based surveys would struggle to reach. By integrating new techniques with traditional approaches, it is hoped that more robust tornado climatologies can be developed that will lead to better predictability for future events.

Tornado Initiation Locations Relative to Surface Heterogeneities and Human Biases

Abstract

The process of tornadogenesis remains poorly understood, and recent literature has put forth a variety of hypotheses for the way that interactions with the heterogeneous land surface could enhance tornadogenesis potential. To examine these hypotheses alongside potential human biases in tornado observations, we retrieved the initiation location for the 452 tornados that occurred in the state of Alabama between 2010 and 2017 from the National Weather Service (NWS) Storm Prediction Center (SPC) SVRGIS database. For each point, we retrieved the underlying elevation, terrain gradients, surface roughness, surface roughness gradients, population density, and road proximity. That distribution was then compared with the same number of random points using Kolmogorov-Smirnov (K-S) tests and logistic regression. All of the variables tested except surface roughness gradients showed statistically significant correlation with tornado locations, but road proximity had the highest K-S score by a wide margin over surface roughness and population density. As a further check, all eight factors were tested as the independent variables of a logistic regression which yielded similar results, with the exception of the fact that surface roughness was not found to be significant in that multivariate context. Although population density is a well-known and significant human bias in the tornado record, these results demonstrate that survey accessibility may be even more important.

Introduction

Tornados are relatively unique among meteorological hazards in that they are constantly in contact with both the cloud base and the Earth's surface. While great strides have been made in the understanding of tornado dynamics and forecast skill in the preceding decades, the influence of surface characteristics remains unclear, particularly as they relate to tornadogenesis. A greater understanding of those influences is important for improving model performance and producing more accurate forecasts. Parsing these extremely complex interactions is further complicated by the need to understand them separately from potential human-induced biases in the historical record that arise from both the reliance on human observation of the storm to report it and the inherent subjectivity of the current rating system.

Laboratory modeling efforts examining the effects of surface obstacles on tornado like vortices date back at least five decades (Dessens 1972), and numerical modelling in computational space continues (Markowski and Dotzek 2011; Lewellen 2012). These studies provide some insight into how topography may affect tornados, but they tend to rely on large eddy simulations with somewhat high result variability and, more crucially, tend to focus on vortices that are already in progress and in contact with the surface. Observational case studies are somewhat prevalent (e.g., Bosart et al. 2006; Bluestein 2000), but are usually limited to a single event. Some studies have attempted to bring together a large number of events to draw conclusions on the particular ways in which tornados are being influenced by terrain and their relative prevalence (Hua and Chavas 2019; Lyza and Knupp 2018). Schneider provides individual examples from the Tennessee Valley for some potential terrain influence mechanisms: (1) valley channeled flow contributing to backing of near-surface winds and locally enhanced storm-relative helicity, (2) vertical stretching of vorticity as storms move over descending terrain,

and (3) upslope flow leading to enhanced updraft strength (Schneider 2009). Intensive observations from the Southern Cumberland Plateau System in Alabama during the VORTEX-SE field project support the notion of orographically enhanced backing and document the presence of lower Lifting Condensation Level (LCL) heights relative to the surface atop the plateau, which can also enhance tornadogenesis potential (Lyza et al. 2020).

In parallel with efforts to understand the influences of underlying terrain, there has recently also been an effort to investigate how surface landcover type could potentially affect tornadic evolution. Changes in landcover type, and the resultant change in surface friction, can be significant sources of horizontal vorticity near the surface that is potentially available to be tilted into the vertical leading to enhanced tornadogenesis potential. There exist numerous theories for the mechanism by which the tilting occurs based on storm environment parameters that are largely outside the scope of this paper (Muncy 2021). Numerical modelling studies have produced mixed results for how vortices encountering obstacles may respond, but seem to indicate that the vortex generation mechanism, strength of the vortex, and location within the vortex all affect whether the obstacle enhances or hinders the strength of the flow (Wang et al. 2017; Lewellen 2012).

Results from observational studies have been similarly mixed. Two recent studies have reported statistically significant relationships between tornado characteristics and surface heterogeneity, but with variations of sign and magnitude in the relationship between either individual cases or geographic subdomain (Houser et al. 2020; Frazier et al. 2019). More recent studies suggest that there is a positive relationship between tornadogenesis and higher roughness values (Muncy 2021). Interestingly, a climatology of tornadoes in Indiana revealed some correlation between land surface type and tornadogenesis locations, based on high occurrences

within 1 km of either urban or forested areas (64% and 42%, respectively); however, the same study noted a marked relation between tornado occurrence locations and population density, highlighting the well documented population density bias in tornado occurrence information (Kellner and Niyogi 2014; Anderson et al. 2007).

Human induced biases in the tornado climatology have been known for decades, and they can arise from a number of factors such as underreporting, the subjectivity of the current rating guidance, and some omission in the very early years of record keeping (Doswell and Burgess 1988; Edwards et al. 2021). The population density bias is one of a number of known human induced biases in tornado climatology, and one that is very well documented in the literature (e.g. Doswell and Burgess 1988; Anderson et al. 2007; Agee and Childs 2014). Because tornados are rated based on damage rather than an empirical measurement, there will always be some ambiguity, but the damage indicators under the Enhanced Fujita scale attempt to create a uniform standard for damage surveys (McDonald and Mehta 2006). Nonetheless, this system still relies on the ability to survey tornado damage, or at least for damage to be noticed in a timely fashion and reported to the local forecast office. As the popularity of storm-chasing as a hobby has increased and survey methods and radar coverage have improved (Edwards et al. 2021), underreporting has decreased, but for operational forecasters conducting official surveys, there are still limitations due to line of sight and time constraints, even when afforded the opportunity to survey outside of populated areas. This leads to the question: are tornado reports biased by accessibility? Most surveys without a specific destination or report are conducted by car, with potential follow-up on foot if damage is sighted. This leads to the possibility of road access as a limiting factor to survey-ability and therefore a bias in the record. This would be especially problematic in rural areas of complex terrain like the highly vulnerable southeastern US (Dixon

et al. 2011). Complicating matters is the fact that roadways tend to follow breaks or contours in topography and land usage.

Parsing all of these competing explanations for distribution of tornado occurrence is a complex and difficult task that is beyond the ability of any one paper. To contribute to that goal, an analysis of Alabama's tornado climatology over eight years is presented here with respect to elevation, elevation slope and aspect, surface roughness, and slope and aspect of surface roughness, as well as population and road access. The distribution for each variable is compared against spatially random distributions to test the potential validity of its underlying hypothesis.

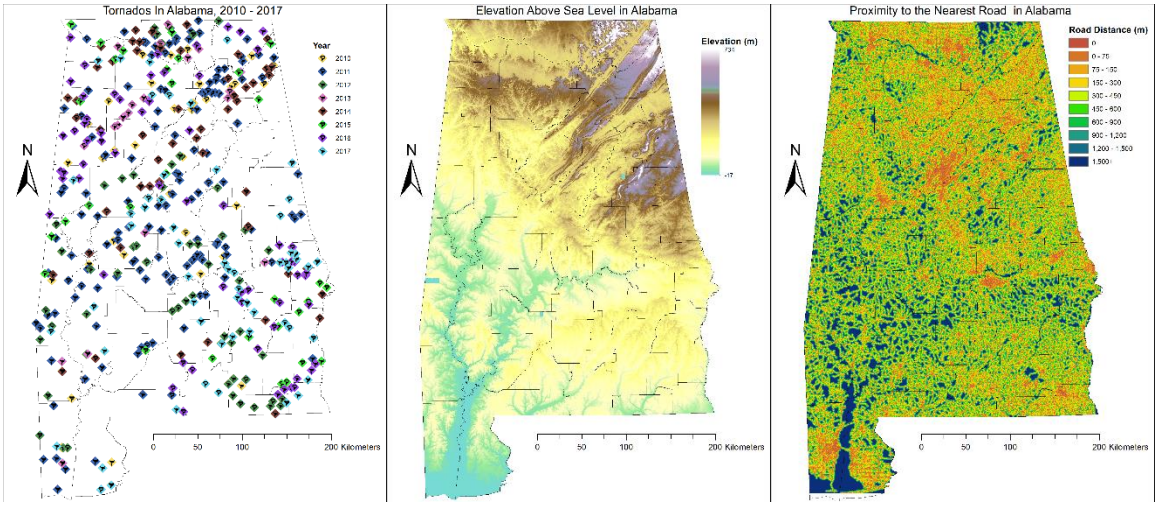

Figure 1: Three panel map of the state of Alabama showing the tornados included in the study alongside elevation and road proximity

Data & Study Area

The state of Alabama is characterized by a diverse mix of land uses and terrain and is situated in the heart of the secondary maximum of tornado occurrence in the United States (Dixon et al. 2011). There are large urban centers in Huntsville, Montgomery, and Birmingham, interspersed with tracks of agriculture and wooded areas. The transition from coastal plain in the south to the Cumberland Plateau in the northeast provides a mix of topographies (Figure 1). These characteristics made it an ideal candidate for this study.

Tornado initiation locations were derived from the National Weather Service's severe weather database (SPC 2018). Relatively recent events were selected to minimize potential biases from survey methodology changes related to the introduction of the Enhanced Fujita Scale in 2007 (McDonald and Mehta 2006). At the time of undertaking the analysis the most recent year for which data was available was 2017. To achieve a sufficient sample size, tornado locations from between 2010 and 2017 were retrieved, yielding 452 individual tornados initiations.

Elevation data were retrieved from the US Geological Survey's National Elevation Dataset 30m resolution (USGS). This resolution was selected to match that of the National Land Cover Dataset (NLCD) that was also used and necessitated mosaicking the individual county levels together. From the statewide raster, slope and aspect were calculated.

Road data was collected from the US Census Bureau's 2019 TIGER/Line files for all the counties of Alabama (USCB 2019a). Based on the types of vehicles commonly available to ground survey teams and the definitions from the Census Bureau, the following road types were selected as accessible for the purposes of this study: 1100, Primary Road; 1200, Secondary Road; and 1400, Local Neighborhood Road, Rural Road, City Street (USCB 2019b). These road types were selected as the types of roads that would be passable for the typical fleet vehicles available to surveyors. From this road network, a Euclidean distance raster was created at 30m resolution. The spatial resolution was chosen for consistency with NLCD data.

Population densities represent block level 2010 census data from the US Census Bureau that have been interpolated to a 60m raster by the USGS (Falcone 2016). This dataset was chosen because its resolution is the closest match to the spatial resolution of the NLCD data of official, available rasterizations.

Table 1: The NLCD class numbers and names and their respective roughness lengths

NLCD Class Number	NLCD Class Name	Roughness Length (m)
24	Developed, High Intensity	1.2
23	Developed, Medium Intensity	0.8
22	Developed, Low Intensity	0.1
21	Developed, Open Space	0.03
82	Cultivated Crops	0.05
81	Pasture/Hay	0.03
71	Grassland/Herbaceous	0.03
41	Deciduous Forest	1.0
42	Evergreen Forest	1.0
43	Mixed Forest	1.0
52	Shrub/Scrub	0.35
90	Woody Wetlands	1.0
95	Emergent Herbaceous Wetlands	0.03
31	Barren Land (Rock/Sand/Clay)	0.015
11	Open Water	0.001

Based on the years of imagery used, the 2011 NLCD release was selected as most representative (Yang et al. 2018). The NLCD data were converted to surface roughness values based on Hirth's values for C-CAP land cover data and NOAA conversion tables (Hirth et al. 2012; NOAA). NLCD classes and their respective surface roughness values are presented in Table 1. Slope and aspect were also calculated for the surface roughness field.

Methods

After preprocessing, eight raster layers were retained, each representing a potential influence on the distribution of tornadogenesis locations: Elevation (Z), Z Slope, Z Aspect, Roughness Length (Z_0), Z_0 Slope, Z_0 Aspect, Population Density, and Road Distance. For the purposes of this study, slope represents the rate of change of a field at a point, and aspect is the compass direction of that change. Each layer is sampled for all of the tornado initiation locations,

yielding a distribution for each of the eight variables (n=452). For comparison, fifty spatially random point distributions (each with m=452) were sampled for each variable as well. A correlation between a particular variable and tornadogenesis should be reflected by that variable's distribution at tornado initiation points differing from a distribution of that variable across spatially random points. This gives the general form hypotheses:

$$H_1: \mathbb{P}_{Torns}(Variable) \neq \mathbb{P}_{Rand}(Variable)$$

$$H_0: \mathbb{P}_{Torns}(Variable) = \mathbb{P}_{Rand}(Variable)$$

The significance of any differences between the tornado and random datasets were assessed using two-tailed Kolmogorov-Smirnov tests where the critical value D for a confidence level c = (1 – α) is given by:

$$D(\alpha) = c(\alpha)\sqrt{\frac{n+m}{n*m}}$$

where *c* is a constant with regards to α and *n* and *m* are the sizes of the two samples (Hodges 1958). For α = 0.01, c = 1.628, which yields a critical value D=0.108292949133 for the sample sizes used (Hodges 1958). The K-S tests were conducted for each variable comparing each random sample to the tornado sample, and subsequently the mean values were calculated across all fifty runs, yielding a single K-S score and p-value for each variable.

As an additional check on the single variable K-S tests and to provide a quantitative measure of directionality of the effects, all eight independent variables were also used as factors in a multivariate logistic regression model.

Table 2: A summary of K-S test means and significance values for all eight variables tested.

Variable	Mean K-S Score	K-S Confidence Level
Elevation	0.14075218	0.0037
Surface Roughness	0.26738944	<0.0001
SR Aspect	0.07995564	0.1361
SR Slope	0.0801327	0.1254
Elev Aspect	0.07146014	0.2735
Elev Slope	0.13331858	0.0096
Population Density	0.19402652	<0.0001
Road Distance	0.41221234	<0.0001

Results

Table 2 illustrates the mean K-S scores for each of the variables tested across the 50 different test runs along with the confidence levels that those scores represent. Five variables met the threshold for statistical significance, all at $p < 0.01$: elevation, elevation slope, surface roughness, population density, and road distance. Neither the aspect of elevation, aspect of surface roughness, nor the slope of surface roughness met the threshold for rejecting H0 at significance levels of 0.1 or better. The largest deviation between two distributions (Figure 2) was found in road distance, followed by surface roughness, population density, elevation, and elevation slope.

Table 3: A summary of logistic regression coefficients and their significance values

	Estimated Coefficient	P-Value
Intercept	-3.721000	< 2.0E-16
Elevation	0.002355	7.86E-06
Surface Roughness	-0.002313	0.477
SR Aspect	-0.000635	0.245
SR Slope	0.001605	0.477
Elev Aspect	-0.000457	0.357
Elev Slope	-0.124200	5.20E-06
Population Density	0.000598	4.53E-13
Road Distance	-0.000704	< 2.0E-16

The results of the logistic regression (Table 3) were largely consistent with those of the K-S tests. The notable exception was that none of the roughness length variables were found to be significant in the multivariate analysis. Because the independent variables were not standardized prior to calculating the logistic regression, the relative magnitudes of the coefficients are not meaningful, but road proximity did exhibit the highest degree of statistical certainty in its correlation with tornado initiation locations.

Discussion

With regards to the elevation variables, four theories for potential terrain influence on tornadogenesis can be examined using the methodology presented here: (1) valley channeled flow contributing to backing of near-surface winds and locally enhanced storm-relative helicity, (2) vertical stretching of vorticity as storms move over descending terrain, (3) upslope flow leading to enhanced updraft strength, and (4) lower ground-relative LCL heights atop terrain minimizing inhibition (Schneider 2009; Lyza et al. 2020). Of these theories, 1 - 3 relate to how the local variation in topography alters local flows, so it would be expected they would present in this methodology as a statistically significant signal for the slope and/or aspect of elevation affecting tornadogenesis. This is the case for slope, but not for aspect, though it is worth noting that for theories 2 & 3, the direction of storm motion, which was not examined here, would highly affect the potential for aspect to play a role. Theory four relies on a function of the value of elevation itself and would present as a significant signal in that variable, which was found to be true. Further, a visual analysis of the distributions (Figure 2) shows that the significant trend is for tornadogenesis to occur at higher altitudes. This provides evidence that the lower ground-

relative LCLs atop Alabama's peaks and plateaus could play a key role in tornadogenesis as previously described (Lyza et al. 2020).

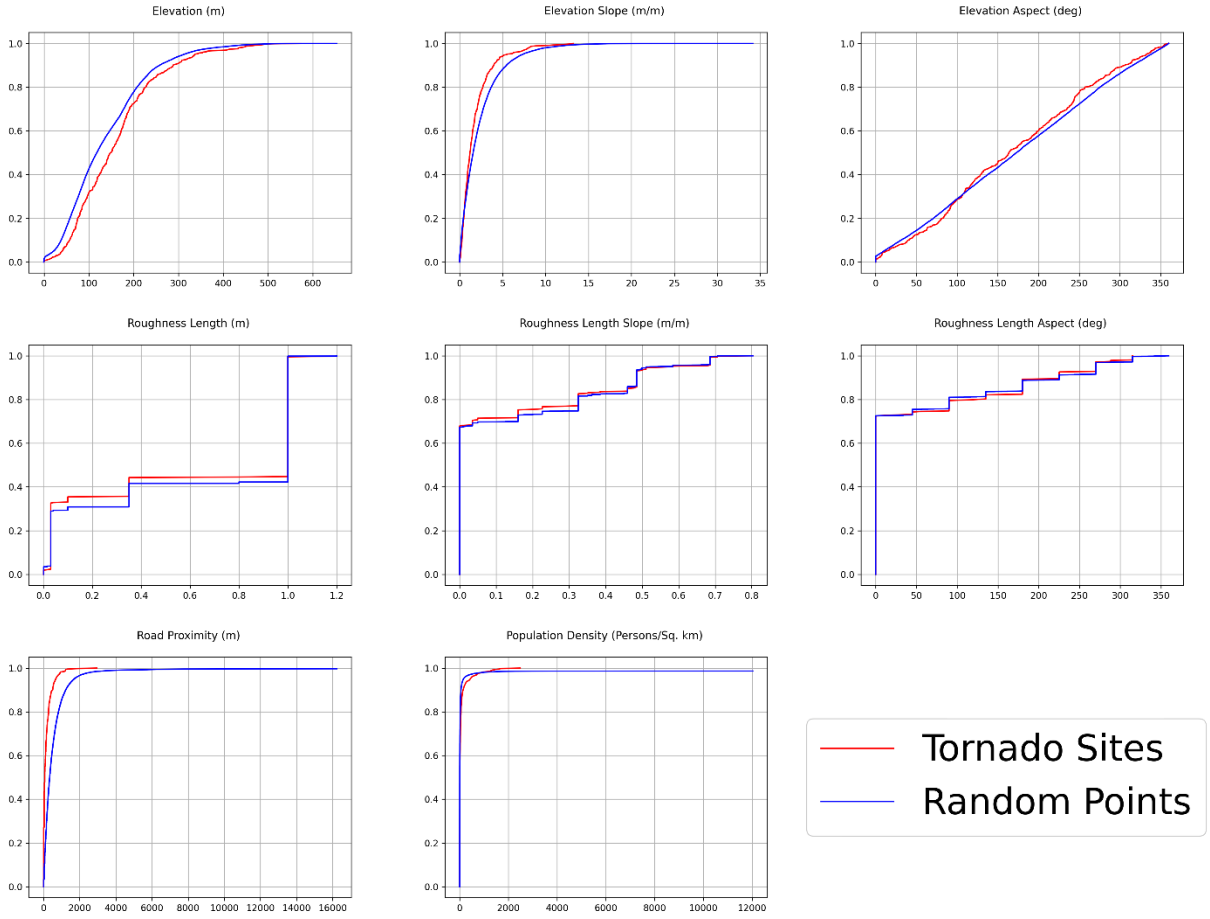

Figure 2: Comparison of the CDFs for all eight variables tested.

Theories related to surface roughness's potential impact on tornadogenesis hinge on the creation of locally higher values horizontal vorticity (and its eventual tilting into the vertical) as storms move across or parallel to gradients in surface roughness (Muncy 2021). This would present as a correlation between the slope and aspect of surface roughness relative to tornadogenesis. That pattern is not evident in this dataset. Instead, there is a statistically significant association with the values of surface roughness themselves, suggesting that certain

land cover types (and therefore roughness values) are more likely to present as damaged and be rated. That said, the analysis of surface roughness effects is subject to the same limitation of omitting storm motion that was true for the elevation gradient analyses, and the notion of surface roughness impacts could benefit from further study in that area.

As expected, the known population bias in the historical tornado record is further demonstrated in the analysis by a statistically significant correlation between population density and tornadogenesis locations (Anderson et al. 2007). Critically however, the road distance metric was far and away the most strongly correlated metric relative to tornadogenesis locations not only among the human-bias variables, but out of the entire study. While it bears repeating that the relative magnitudes of K-S scores are not necessarily directly proportional representations of influence, it is also extremely noteworthy that the road distance metric introduced here has more than double the K-S score of the benchmark known bias, population density. In visual examination it is also the most starkly different distribution with tornados initiating overwhelmingly more closely to roads than random chance would predict.

The results of the logistic regression model largely support the conclusion that road proximity is a large potential bias in tornado climatology. Further, the magnitude and direction of the elevation and elevation slope coefficients lend support to the ideas that tornados are potentially (1) more likely to form atop higher terrain or (2) in areas of descending terrain due to lower ground relative LCL heights and enhanced vertical stretching of vorticity, respectively. The lack of statistical significance in the surface roughness factors in the multivariate analysis as compared with the same signal in the univariate analysis is consistent with the idea that the univariate signal was a byproduct of interdependence between surface roughness and another independent variable. This could be for a number of reasons, such as the use of shelterbelts

between types of land use (e.g. between the edge of a field and a road), the difficulty of certain types of development in more complex terrain, or the fact that roads tend to follow contours of human development as well as terrain. The fact that the other factors such as elevation, elevation slope, population density, and road proximity remain significant under multivariate scrutiny while surface roughness does not however, demonstrates that those other factors are more likely to be the true drivers.

Conclusion

The results of this study with regards to terrain and land cover influences underscore the importance of incorporating storm direction into future discussions on orographic and frictional effects, and especially the need for studies that do this with large sample sizes. Recent extensive field work in the Southeastern United States, such as PERiLS, should also prove fertile ground for further validation of the lowered ground-relative LCLs atop various terrain features across different storm environments.

The results of the K-S testing for human-induced biases suggests that in an age of increasing documentation of tornados, proximity during the event is much less a factor in the bias of the dataset (and therefore our assumptions about the tornadogenesis process) than the ability to see and reach the site of tornadogenesis after the fact. Fortunately, technologies such as UAS imagery and commercial satellite imagery at higher spatial and temporal resolutions are increasingly available to expand the ability of surveyors to see and document damage in areas far removed from roads (Kingfield and de Beurs 2017; Wagner et al. 2019). Further research on corrective factors for accessibility bias in the vein of the work already done on population bias (Anderson et al. 2007) or methodological changes (Edwards et al. 2021) would also be beneficial. The interconnected nature of the road networks and the topography underlying

prevailing theories about surface effects may have broad implications for the production of robust tornado climatologies and understandings of tornadogenesis going forward.

Tornadic Damage Detection Using a Sentinel-2 Derived Disturbance Index

Abstract

Recording the historic occurrences of tornados provides important data for understanding of tornadic processes and ultimately benefits public safety, infrastructure resilience, and forecasting. This information is typically gathered by National Weather Service (NWS) personnel through extensive ground surveys of the affected areas. This process is constrained by operational budgets and staffing requirements and is subject to potential observation bias and the contamination or removal of debris fields in short time frames post-event. In order to improve the accuracy of the tornado record, we assessed the viability of using Sentinel-2 derived disturbance index imagery for detecting tornado damage. We retrieved surveyed location and intensity data for fifty tornados that occurred within 14 scenes that totaled approximately 560,000 sq km. The mean disturbance index (DI) was calculated for each scene as a whole and individually for the different landcover types within each scene. The mean of these DI values was compared to their underlying EF damage rating using a Spearman rank correlation. Additionally, we constructed receiver-operator curves for each combination of landcover and EF rating to examine the predictive value of DI in a variety of situations. The results demonstrate that while DI is useful for detecting swaths of tornadic damage, its utility is highly landcover dependent. Wooded areas and wetlands performed best, which is in line with the design of DI as an indicator of forest disturbance. Additionally, we found that Sentinel-2 does not provide an appreciably lower intensity threshold for damage detection than previously described (e.g., Molthan et al. 2014; Kingfield and de Beurs 2017), but does have operational benefits, such as increased revisit frequency and higher resolvable detail in damage areas.

Introduction

In order to develop and maintain a record of tornado occurrence, the National Weather Service traditionally conducts ground surveys in the immediate aftermath of tornadic events alongside aerial surveys for some larger scale events (Kingfield and de Beurs 2017). These surveys generate the tornado climatology, which is the historical record of where and when tornados have occurred and with what intensity. This information informs our understanding of tornadic processes and by extension: infrastructure and ecosystem resilience (Kingfield and de Beurs 2017; Wagner et al. 2012), public safety and risk management (Walsh and Tezak 2013; Ramsdell et al. 2007), and forecast validation (Speheger et al. 2002; Witt et al. 1998). It is therefore in the best interests of science and the broader public that as many tornados as possible are surveyed as thoroughly and as accurately as possible. To help achieve this goal, we developed and evaluated a novel technique for detecting tornado damage swaths based on satellite remote sensing.

Unfortunately, time sensitive damage indicators, budgetary and personnel constraints (Doswell and Burgess 1988; Doswell et al. 2009), and underreporting (Shikhov and Chernokulsky 2018; Anderson et al. 2007) combine to mean that many tornado surveys are either incomplete or never conducted at all. The current system relies on NWS personnel being available to perform survey duties without affecting staffing in such a way that would compromise the ongoing forecast mission. They have a short window of time in which to work before potential damage indicators will be changed or removed altogether. Frequently, this means that they are required to prioritize areas with known damage, which can introduce bias in areas where damage may go unnoticed until the survey period is over. The result is a climatology that is, somewhat understandably, biased towards the areas of peak intensity that define a tornado's

rating and the human developments that a given tornado impacts (Shikhov and Chernokulsky 2018; Kingfield and de Beurs 2017). To help reduce this bias, additional data on tornado damage collected over broader spatial extents is needed.

Spaceborne remote sensing has been put forward as a potential remedy for some of the gaps in more traditional survey methods. Earth-observing satellites collect gridded data consisting of surface reflectance in the visual and infrared wavelengths. Many satellite missions are global in scope with revisit times of days to weeks, which facilitates the rapid acquisition of data following tornado events (Claverie et al. 2017). Previous studies have utilized a variety of sensors and methodologies to detect damage from severe thunderstorms (Bell 2019). Most have utilized the Normalized Difference Vegetation Index (NDVI), which is a spectral index based on the red and near infrared wavelengths that is used to diagnose vegetation health. With the combined use of the MODIS and Landsat ETM+ sensors, this approach has produced robust results, detecting tornados down to the EF1 level depending on landcover (Molthan et al. 2014), even outside of vegetated environments (Jedlovec et al. 2006; Shikhov and Chernokulsky 2018). Analysis using NDVI is limited by the fact that it can be highly sensitive ground moisture content, which is understandably variable between pre and post storm environments. Previous applications of NDVI for tornado damage assessment have also used a change detection approach, in which post-storm conditions must be evaluated relative to a before-storm baseline NDVI, which requires cloud free satellite overpasses in relatively close succession before and after the event (Singh 1989; Kingfield and de Beurs 2017).

More recently, researchers have sought to employ a different set of spectral indices known as Tasseled Cap (TC) indices (Crist 1984). TC indices are a robust and computationally efficient way to monitor vegetative health and broader landcover change and can be thought of as

broadly similar to the physical concepts of albedo (brightness), photosynthetic activity (greenness), and surface moisture (wetness) (Shi and Xu 2019; Dwomoh and Wimberly 2017). TC indices represent a significant improvement over NDVI for the purposes of disturbance detection because they are able to give a more complete picture by utilizing a combination of six visual, near infrared, and shortwave infrared bands rather than two that are used in NDVI. The disturbance index compares each of the tasseled cap indices to undisturbed reference values of that index of the same land cover type throughout a single image (Healey et al. 2005). In this way, it is possible to generate a meaningful disturbance metric from a single post-event image (Karstens et al. 2013; Kingfield and de Beurs 2017). Previous studies were limited to the 30m resolution of Landsat ETM+ imagery which has since been surpassed by the 10-20 m spatial resolution by Sentinel-2. The recent derivation of tasseled cap transform coefficients for Sentinel-2 means that it is possible to assess the effects of that increased spatial resolution on the detectability of tornado damage using the disturbance index technique (Shi and Xu 2019).

This study seeks to evaluate the ability of high-resolution Sentinel 2 imagery to detect tornadic damage signatures as well as explore the possibility of utilizing that imagery to classify damage across a variety of land cover. The specific objectives are to: 1) calculate Sentinel-2 disturbance index values for tornado impacted areas including a wide variety of intensities, path widths, and landcover types; and 2) compare the disturbance index with traditional survey data to determine the applications and limitations of remotely sensed tornado damage detection.

Data & Study Area

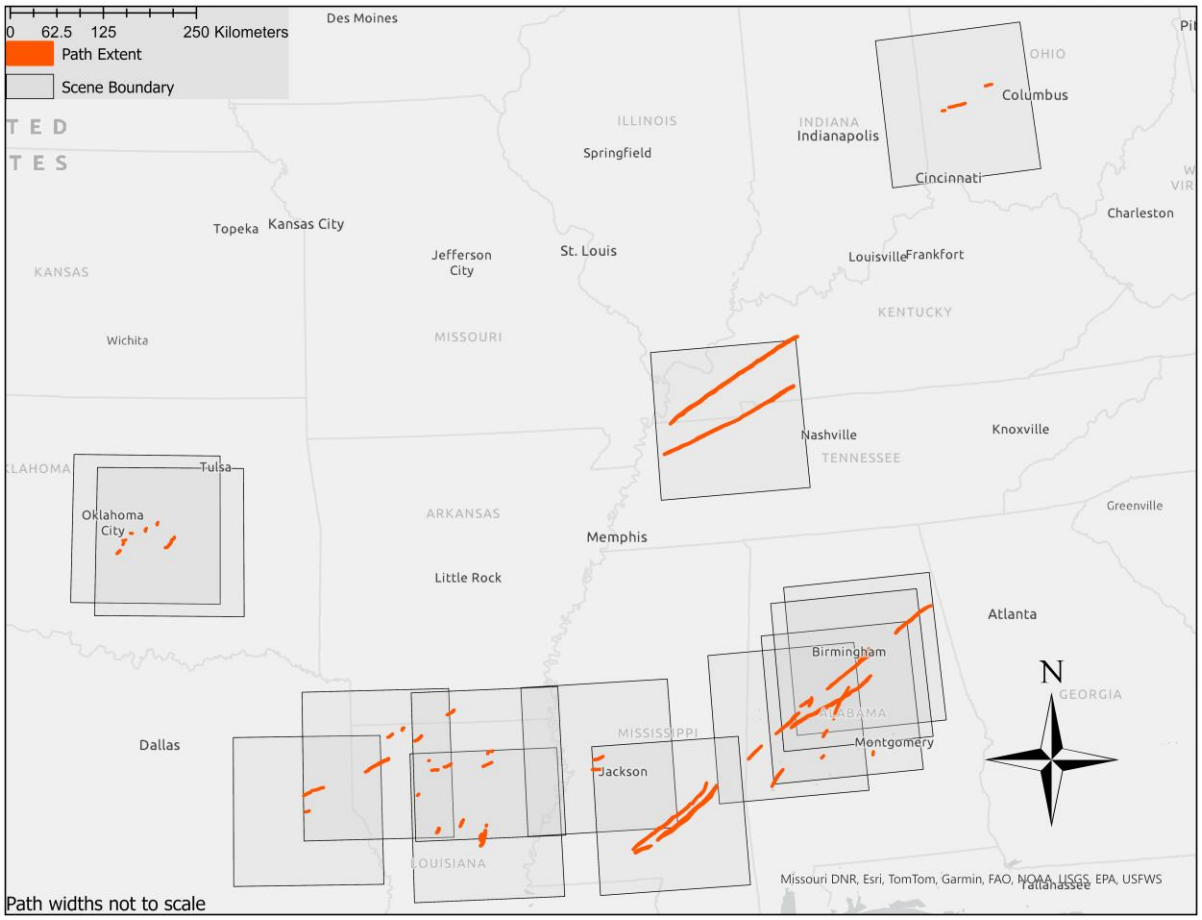

Figure 3: Study location map showing all fourteen scene boundaries and the path extent of the fifty tornados. A wide variety of landcover types, geographic locations, path characteristics, and event timings are represented.

In order to assess the diagnostic utility of high-resolution Disturbance Index (DI) imagery for tornado damage, fourteen cases were selected, each of which was used to construct a scene centered on a path of interest and containing at least one surveyed tornado path. To be eligible for selection, the survey must have recorded the varying intensities as nested polygons within the overall path rather than the alternative method that applies the maximum intensity to the whole extent of the path. The cases were selected using a combination of the National Weather Service (NWS) Damage Assessment Toolkit (DAT) and the NWS Storm Prediction Center's (SPC) SVRGIS tornado path dataset (NOAA; SPC 2018). The tornados also needed to have occurred

after 23 June 2015, as that is the first date for Sentinel 2 Top of Atmosphere Reflectance data in the Google Earth Engine catalog. From there, cases were subjectively chosen to present a diverse range of path widths, geographic locations, and traversed land cover types. For each of the selected fourteen cases, a scene was constructed in a 200 km x 200 km square centered on the midpoint of the associated path. All other tornados occurring on the same UTC date were also included, yielding a total of fifty tornados. The nested intensity features bring the total number of intensity patches across all fourteen scenes to 258. The total area for each intensity level is displayed in Table 4.

Table 4: List of sampled cases sorted by date and including the scene centroid and the distribution of tornado-disturbed area by damage class

Date	Central Latitude	Central Longitude	Tornado Damaged Area (Square Kilometers)					
			EF0	EF1	EF2	EF3	EF4	Total
2 April 2017	31.755	-92.159	11.95	64.09	0.70	0	0	76.73
13 April 2018	32.530	-93.683	47.54	10.42	0.02	0	0	57.97
21 May 2019	35.403	-97.021	6.24	0.38	0.01	0	0	6.63
12 April 2020	32.492	-92.106	3.42	3.41	0.73	0.11	0	7.67
12 April 2020	31.742	-89.557	149.65	207.82	93.67	30.52	2.17	483.84
25 March 2021	33.310	-86.804	120.99	136.67	51.57	2.89	0	312.12
10 December 2021	36.467	-88.246	186.03	257.68	180.93	22.21	2.98	649.84
3 February 2022	32.746	-87.786	33.56	23.31	5.71	0	0	62.58
17 February 2022	33.490	-86.593	3.01	2.47	0	0	0	5.48
22 March 2022	32.501	-90.520	9.09	3.96	0.12	0	0	13.17
30 March 2022	32.928	-86.991	33.35	16.45	7.62	1.52	0	58.93
4 May 2022	35.251	-96.668	9.32	2.96	0.23	0	0	12.51
5 May 2022	31.988	-94.684	6.67	9.50	1.07	0	0	17.24
8 June 2022	39.981	-84.233	6.97	3.57	0	0	0	10.54
Total			627.79	742.68	342.36	57.25	5.15	1775.24

Methods

For each case, Sentinel-2 top of atmosphere imagery was collected and processed using Google Earth Engine (Gorelick et al. 2017). The Sentinel-2 program consists of a constellation of

two satellites, each carrying a Multi-Spectral Instrument (MSI) payload recording imagery across 13 spectral bands (see Table 5) and a revisit time of ten days for each satellite or five days for the constellation. Harmonized, top-of-atmosphere imagery was retrieved for a period of 37 days post-event. The individual images were filtered to include only those with cloud percentage less than 5% and the remaining clouds were masked using the cloud data provided with the imagery. Where there were multiple images at the same point, median pixel values for each band were used to derive a single image.

Table 5: Sentinel band summary with central wavelength, bandwidth, and spatial resolution

Band Number	Band Descriptor	Central Wavelength (nm)		Bandwidth (nm)		Pixel Size (m)
		Sentinel 2A	Sentinel 2B	Sentinel 2A	Sentinel 2B	
1	Aerosols	442.7	442.3	20	20	60
2	Blue	492.7	492.3	65	65	10
3	Green	559.8	558.9	35	35	10
4	Red	664.6	664.9	30	31	10
5	Red Edge 1	704.1	703.8	14	15	20
6	Red Edge 2	740.5	739.1	14	13	20
7	Red Edge 3	782.8	779.7	19	19	20
8	NIR	832.8	832.9	105	104	10
8A	Red Edge 4	864.7	864	21	21	20
9	Water vapor	945.1	943.2	19	20	60
10	Cirrus	1373.5	1376.9	29	29	60
11	SWIR 1	1613.7	1610.4	90	94	20
12	SWIR 2	2202.4	2185.7	174	184	20

Once the images were processed, we utilized the transforms derived in Shi et al., 2019 to calculate the Tasseled Cap (TC) indices of Brightness, Greenness, and Wetness, from bands 2, 3, 4, 8, 11, and 12, handling resolution differences within the Google Earth Engine with nearest neighbor resampling. The utility of TC indices is extended by computing the Disturbance Index, which allows for the assessment of forest disturbance from a singular image by rescaling the TC indices for a given pixel to the image wide mean and standard deviation for that pixel's given

landcover type and then combining the three rescaled values into a single index (Healey et al. 2005). For example, to compute the TC brightness B_r is

$$(1)\ B_r = \frac{B - B_\mu}{B_\sigma}$$

where B is the brightness at the pixel, B_μ is the mean brightness for that pixel's landcover type, and B_σ is the standard deviation of brightness across that landcover type. Having repeated that process to compute the TC greenness, G_r, and TC wetness, W_r, the DI can be computed as

$$(2)\ DI = B_r - (G_r + W_r)$$

The mean Disturbance Index for each intensity level (EF-0 through EF-4) was calculated for each scene from a sample of 2000 pixels per class for each image (or all where <2000 were available) as well as for the areas with no tornado damage (designated intensity level -1). In addition to the whole scene, the same analysis was conducted after applying a mask to the water pixels, and separately for each of five general land cover categories: open water; barren or developed land; grasses, shrubs, and agriculture; forests; and wetlands. These general classifications were derived from the NLCD classes (see Table 6) and are intended to discern possible performance differences related to the vegetation-focused nature of the DI (Homer and Dewitz 2018). An example of the DI in relation to two tornado tracks that occurred in 2017 in nearby but dissimilar landcovers is shown in Figure 4. Tornado A is an EF2 that occurred west of Cooley in an area of wetland and evergreen forests. Tornado B is an EF2 with a similar path size to the one that occurred in the suburbs of Alexandria. Tornado A is very clearly defined for most of its track through decay whereas Tornado B is very poorly resolved for any of its track.

Table 6: Summary of the reclassification scheme that was used to generate the simplified landcover types. It is intended to group classes by their expected response to the DI.

NLCD Class Descriptor	NLCD Class No.	Simplfied Class Number	Simplfied Descriptor
Open Water	11	0	Water
Developed, Open Space	21	1	Developed or barren
Developed, Low Intensity	22	1	Developed or barren
Developed, Medium Intensity	23	1	Developed or barren
Developed High Intensity	24	1	Developed or barren
Barren Land (Rock/Sand/Clay)	31	1	Developed or barren
Deciduous Forest	41	3	Forest
Evergreen Forest	42	3	Forest
Mixed Forest	43	3	Forest
Shrub/Scrub	52	3	Forest
Grassland/Herbaceous	71	2	Grass, shrub, and agriculture
Pasture/Hay	81	2	Grass, shrub, and agriculture
Cultivated Crops	82	2	Grass, shrub, and agriculture
Woody Wetlands	90	4	Wetlands
Emergent Herbaceous Wetlands	95	4	Wetlands

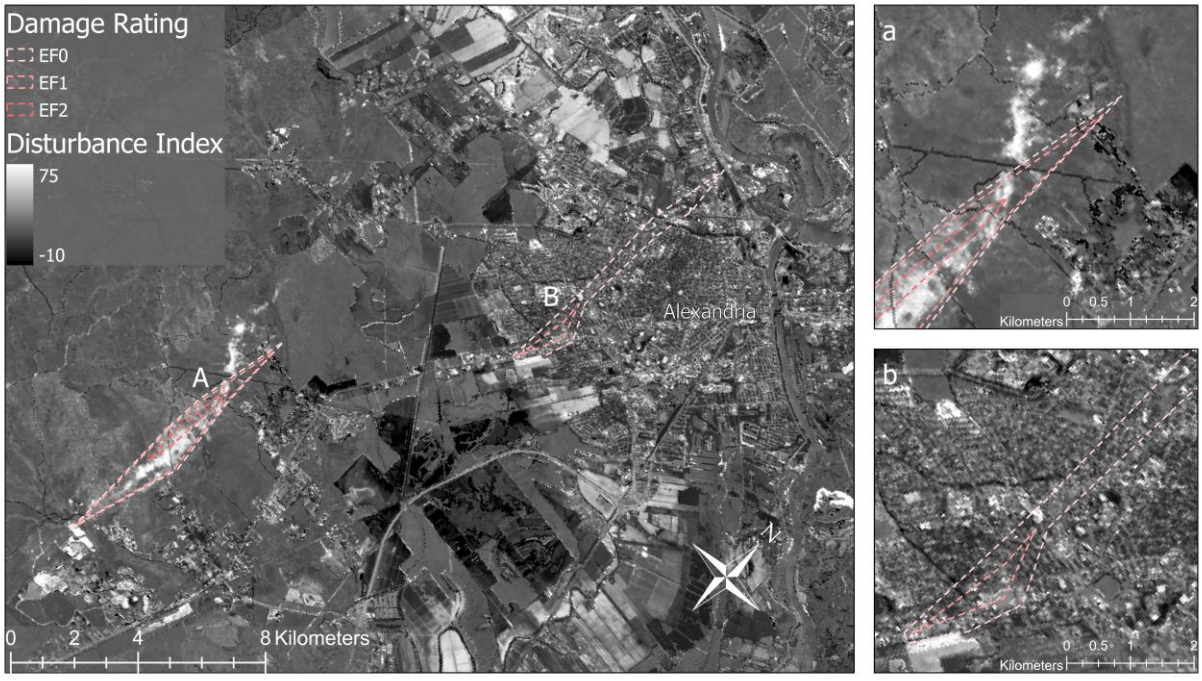

Figure 4: A map showing two tornados that occurred very closely in time and space but are resolved very differently by the disturbance index.

The strength of the association between the DI and the ordinal levels of tornadic damage was assessed by calculating Spearman rank correlation coefficients between the DI and levels of intensity. Additionally, receiver operating characteristic (ROC) curves were generated to characterize the discriminatory power of the DI for binary classification of tornadoes at each intensity level. These curves plot the proportion of true and false positives all possible values of DI. The ROC analysis was performed for the complete dataset, the water masked dataset, and for each of the aforementioned simplified landcover classes.

Table 7: Spearman rank correlation coefficients of the relationship between EF rating and disturbance index for each landcover class and the overall dataset with and without water mask.

Landcover Class	Spearman's ρ
Overall	0.31744
Overall, Excluding Water	0.32101
Open Water	0.01907
Barren & Developed Land	0.20391
Grasses, Shrubs, and Agriculture	0.15361
Forests	0.38241
Wetlands	0.33637

Table 8: A summary of the results generated across the entire dataset for each landcover type and damage intensity pair as well as for intensity across all landcover types.

	Overall	Overall, Excl. Water	Open Water	Barren & Developed Land	Grasses, Shrubs, and Agriculture	Forests	Wetlands
	Mean (Std Dev)	Mean (Std Dev)	Mean (Std Dev)	Mean (Std Dev)	Mean (Std Dev)	Mean (Std Dev)	Mean (Std Dev)
Background	-0.0362 (2.32)	-0.0524 (2.3)	0.0374 (1.81)	-0.0365 (2.52)	-0.0314 (2.4)	-0.0104 (2.29)	-0.0432 (1.94)
EF0	0.0753 (2.35)	0.0475 (2.35)	0.223 (1.92)	0.193 (2.46)	-0.292 (2.36)	0.274 (2.31)	0.298 (2.24)
EF1	0.518 (2.52)	0.508 (2.51)	0.194 (1.85)	0.472 (2.5)	0.118 (2.35)	0.778 (2.48)	1.01 (2.62)
EF2	1.75 (2.68)	1.78 (2.68)	0.164 (1.71)	1.39 (2.38)	0.664 (2.33)	2.12 (2.71)	2.19 (2.96)
EF3	2.96 (2.62)	2.98 (2.67)	0.372 (2.01)	2.04 (2.59)	1.41 (2.39)	3.53 (2.64)	4.39 (2.58)
EF4	2.84 (3.27)	2.8 (3.28)	3.36 (1.49)	0.705 (2.64)	1.84 (2.58)	4.74 (2.97)	6.59 (1.99)

Results & Discussion

Overall, the results of our study indicate that there is some utility in disturbance index information derived from higher resolution satellites for the purposes of tornado damage detection, but that the results are highly dependent on land cover type. This is to be expected given the specialized applications for which the disturbance index was developed (Healey et al. 2005). All categories demonstrated a positive correlation between the DI and tornado rating, although to varying degrees (Tables 6 and 7, Figure 5).

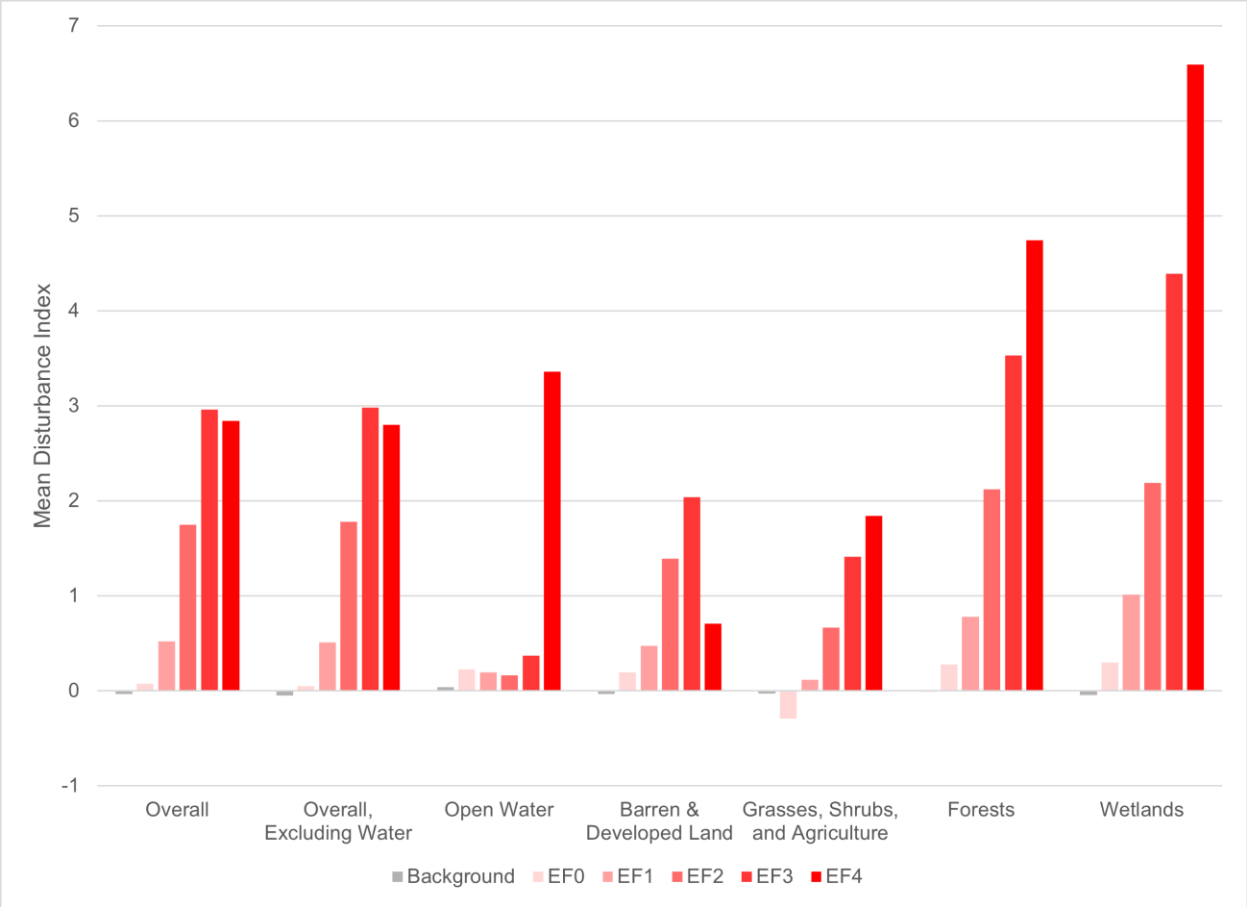

Figure 5: A bar chart showing the mean DIs for each landcover type at each intensity level. Moving left to right across categories and within categories across intensities, the mean DIs tend to increase

As expected, open water areas had the weakest correlation with a Spearman statistic very near zero. Any appreciable relationship is likely due to the changes in water levels. Barren or

developed land, and the overall dataset both had higher average DI values in areas of EF3 rather than EF4 damage, possibly suggesting a threshold at which increasing damage is either less likely or becomes less detectable in those environments. Wetland and forest landcover types both exhibited expected behavior with regards to having relatively high detectability with the DI and relatively consistent transitions through each damage regime. Notably, with the exception of open water, the standard deviation was high relative to the actual values of DI for all land cover types and damage intensities when the data were analyzed at the pixel scale. The standard deviation tends to be between 2 and 3, and that trend is consistent at other subsample sizes.

Table 9: The area under the receiver operator curve (AUROC) values for the overall dataset with and without water masking, and for the individual landcover types. Values higher than 0.5 represent outcomes better than random chance.

	Overall	Water Masked	Open Water	Barren & Developed	Grass, Shrub & Ag	Forests	Wetlands
≥ EF0	0.612	0.611	0.512	0.585	0.532	0.647	0.643
≥ EF1	0.653	0.656	0.505	0.606	0.588	0.689	0.686
≥ EF2	0.731	0.734	0.521	0.667	0.641	0.775	0.761
≥ EF3	0.761	0.761	0.501	0.670	0.686	0.825	0.880

Similar trends are present in the area under the receiver operator curve (AUROC) analyses (Table 9). An AUROC value greater than 0.5 represents predictive value better than random chance. Appropriately, open water which should not exhibit tornado damage, has values very close to 0.5. The detectability for the other landcover types appears to be largely the same as in the means-based analysis. Across all landcover types except wetlands, AUROC values generally have the largest increase between EF1 and EF2, suggesting that the lower bound on detectability lies in that range of damage intensities.

High-resolution satellite imagery appears useful for the problem of tornado damage detection, but its utility is situation based on landcover type and the sensitivity appears to be limited by high variability regardless of resolution. This is consistent with the inherent

shortcomings of applying a particular index in a 'one-size-fits-all' manner, and it is consistent with previous works that have described similar limitations in minimum threshold of detectability. For instance, Jedlovec et al., 2006 were able to detect tornados down to F2 from examining the 250-meter resolution visual and NIR bands of MODIS imagery from before and after a storm in forested areas and could detect additional features when using a 16-day composite NDVI. When increasing resolution to the 15-m and 30-m data from ASTER and Landsat, respectively, they found that they could detect some F1 tornado damage, but that it was highly variable based on swath size, landcover, and seasonality.

Our results saw that the largest jump in discriminatory skill came between the EF1 and EF2 classifications. These results are similar to those presented in Molthan et al. 2014, where single day NDVI derived from 30 m Landsat imagery yielded a detection success rate of 32.4% across all intensities, but 65.6% when only tornados ≥EF2 were considered. The similarity between our results and results from previous studies using lower resolution imagery suggests that an increase in spatial resolution does not necessarily yield a decrease in minimum detection threshold. The relatively high standard deviations across all tests indicate that the additional resolution may actually be introducing more noise than useful information to the analysis. Figure 6 is a box and whisker plot with outlying points removed that demonstrates the large intra-class variability and considerable overlap between damage intensities. Although the minimum threshold for detection appears to be relatively unchanged by moving to higher resolution imagery, the increase in spatial detail of the damage swaths that are detected can still provide useful insight into the variability of damage among similar damage indicators and different parts of the storm.

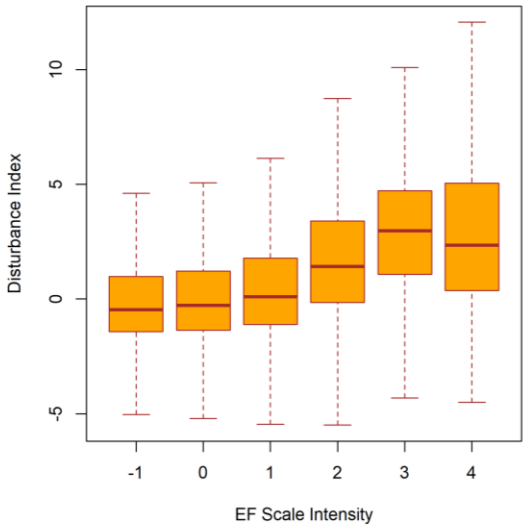

Figure 6: A box and whisker plot with outliers removed for DI values sorted by EF scale intensity. The significant overlap between damage classes even within the center quartiles is a key challenge for damage detection is represents a major obstacle for classification

Another major issue that simple DI analyses presents for detecting tornadic damage is that it is highly dependent on the landcover that is being damaged. Figure 4 shows two tornados that occurred over completely different types of land cover, but on the same day in very close proximity to each other. The difference between how well they are resolved by the DI is much larger than the difference of their one EF grade separation would suggest. Even in areas that are rated the same, the EF0 and EF1 portions of each track, tornado A, which occurred over a mix of evergreen forest and wetlands, is much more well defined than tornado B that occurred in the developed area around Alexandria. Even within landcover classes, the variance in responsiveness to DI can vary greatly. This is especially true in the 'developed and barren' and 'grass, shrub, and agriculture' classes as the percent of tree cover can vary widely in those classes. This is not wholly discouraging for the use of DI as a supplemental tool for tornado surveys however, because the tornados most frequently underreported are in less populated and more difficult to access areas (Anderson et al. 2007; Shikhov and Chernokulsky 2018). Because the underlying spectral indices are geared towards vegetation, the DI method works very well in just the kinds

of areas that traditional surveys have difficulty with like deep forest and wetlands. This is partially demonstrated by tornado A, where the dissipating portion of the track appears to be more well resolved in the DI based assessment than the ground survey polygons.

Disturbance index works best in forested landcovers by design, by taking advantage of the fact that brightness levels tend to increase while wetness and greenness levels tend to decrease when a forest is disturbed. In figure 7, the component indices can be seen to demonstrate this where two tornados crossed through the Oakmulgee Wildlife Management Area near Centreville, AL on March 25, 2021. Brightness increases rather significantly along both tracks while greenness and wetness decrease sharply.

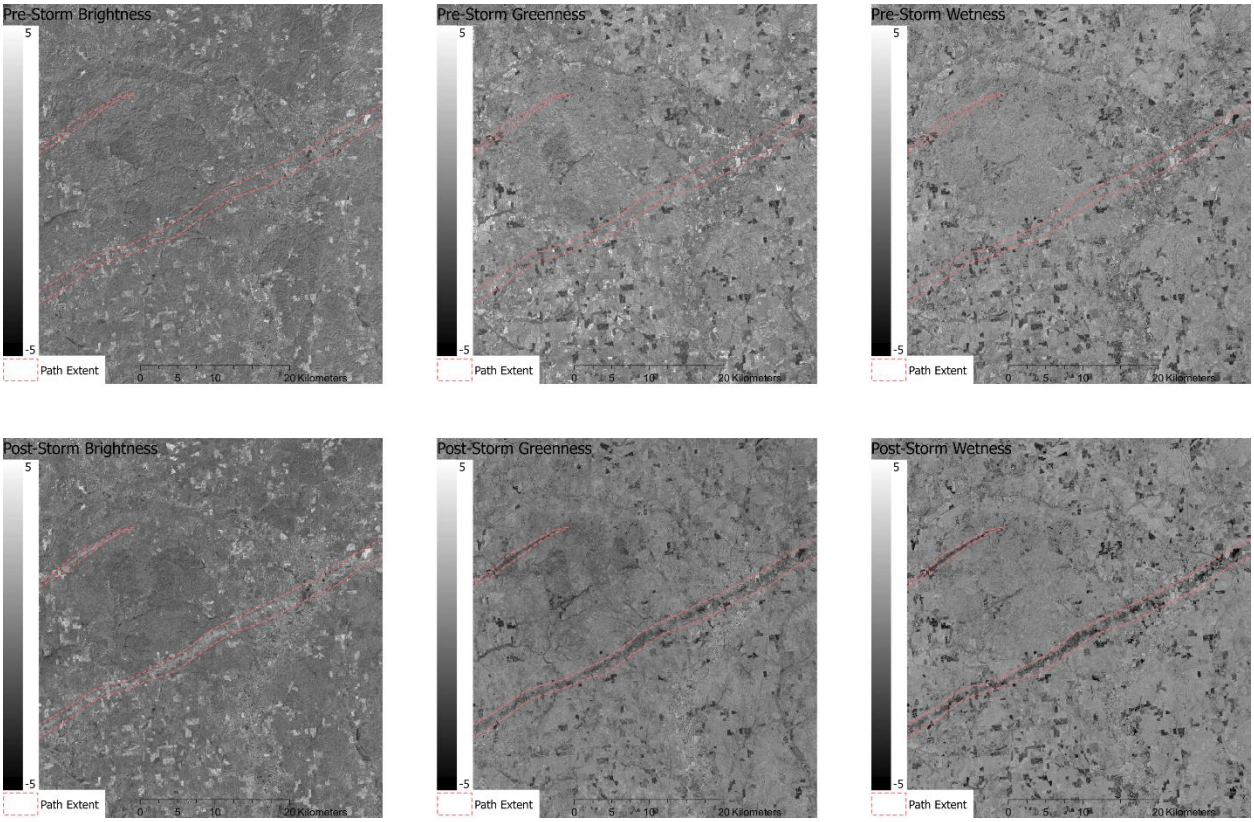

Figure 7: Before and after plots for each of the three tasseled cap index components for two tornados that occurred on March 25, 2021, in a managed forest near Centreville, AL. The images show values that have already been normalized to the background values for their landcover type, and are the values directly ingested into the DI formula.

This focus on a specific spectral response is also why extending the DI to other land classes yields relatively poor results. The goal of this research was to evaluate the utility of this specific disturbance index for the problem of tornado damage detection, but previous work has demonstrated how the DI can be adapted to other landcover types by examining their spectral response to disturbance (de Beurs et al. 2016).

Figure 8: Histograms comparing the distribution of values for each component TC index and the DI for areas impacted by tornado damage rated EF-2 or greater.

Figure 8 explores the spectral response for pixels impacted at intensity EF-2 or greater across the non-water landcover classifications used in this study. The main cause of poor performance (i.e. minimal difference before to after the storm) in the barren and grass categories appears to be the low sensitivity of wetness. The disparity between pre- and post-event values in greenness is also smaller in those areas, but there is much less overlap in the distributions than for wetness. Brightness tends to increase in barren and developed areas and forests, while it tends to remain close to the same in grassland, shrubland, and agricultural areas and in wetlands. With the exception of brightness, these broadly match the trends presented in previous work applying

a DI to grasslands (de Beurs et al. 2016). The difference in brightness behavior could be a function of soil properties, which were not evaluated here.

Examining change cause by disturbance has been shown to improve the performance of an adapted DI in fire severity assessment (DaSilva et al. 2021). In order to explore whether a differencing approach could alleviate the persistent high values present in urban areas to improve detection in the Alexandria example (Figure 4), we subtracted the DI computed based on images in a 37 day post event window from the DI calculated for a the window extending up to 37 days prior to the event.

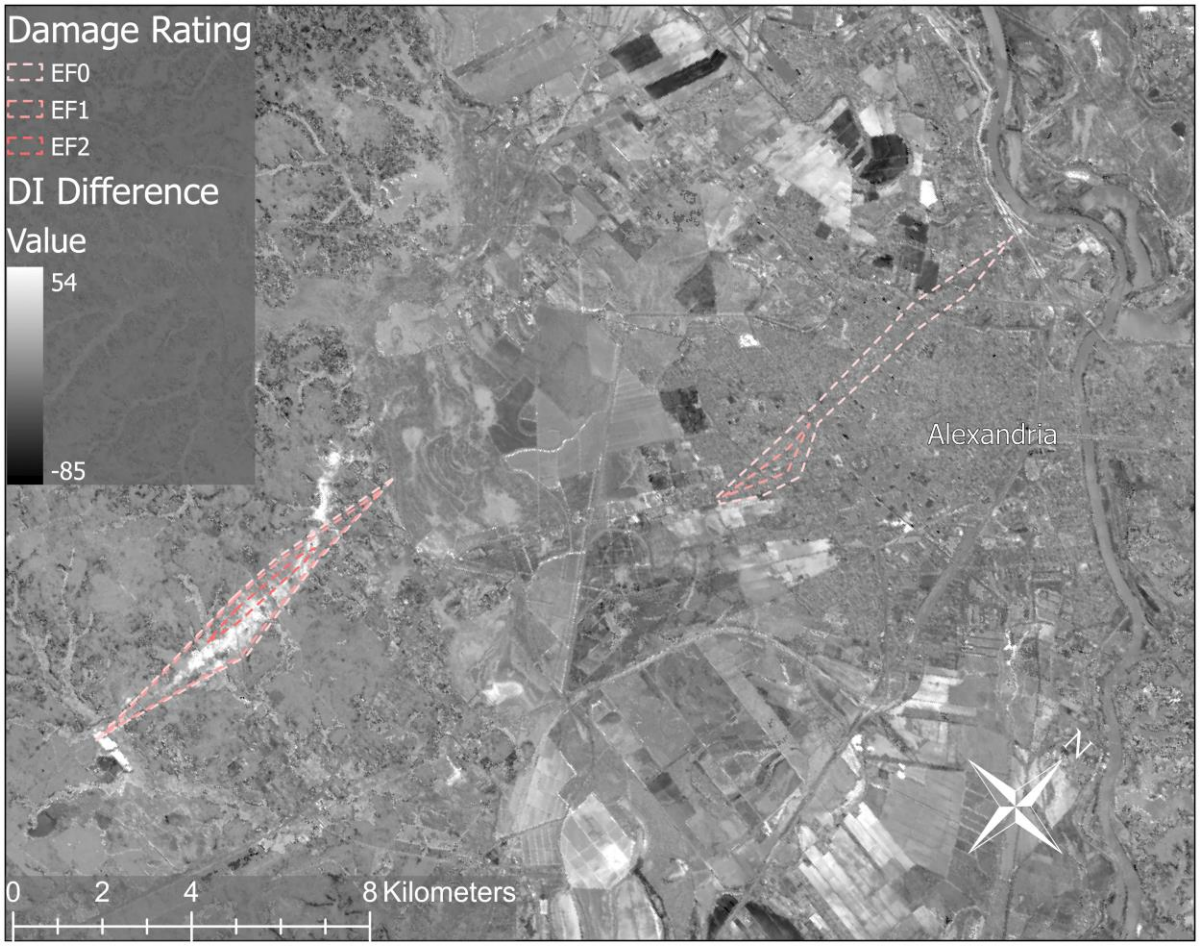

Figure 9: The difference between post-storm and pre-storm DI for two tornados near Alexandria on 2 April 2017.

The differencing technique had the desired effect of reducing most of the persistent high signals in the urban areas of Alexandria, but unfortunately there was not enough damage signal remaining to be visible (Figure 9). While this technique may improve resolvability around smaller obstacles in an already defined path, it seems that a more tailored DI for urban areas based on their spectral response would be required to significantly improve performance.

As more imagery with higher spatial and temporal resolution becomes available to surveyors and technologies like machine learning progress in their ability to discriminate damage indicators in it, these topics should be revisited. Because the underlying damage scale is tied to individual damage indicators, a classification scheme that involves identifying degradation of particular indicators could be feasible at higher resolutions and with adequate data on the locations and types of damage indicators in a given area. More feasible in the short term may be the development of additional indices for use human-made or barren land covers that have little or no photosynthetic activity to try to improve tornado detectability in these land cover types. Additionally, more accurate comparisons could likely be made across vegetated or partially vegetated areas by including tree cover as part of the classification to reduce intra-class variance in DI responsiveness. Teaming these approaches with an edge detection method would likely reduce the large intra-class variability and would be ideal for determining outer track boundaries.

Conclusion

Recent literature has suggested several ways that surface heterogeneities may enhance tornadogenesis potential including enhanced low level convergence at the boundaries between land cover type (Kellner and Niyogi 2014; Frazier et al. 2019), enhanced updrafts along upward sloping terrain and vertical stretching of vorticity along negatively sloping terrain (Schneider 2009; Hua and Chavas 2019), lower ground relative LCL heights at higher elevations, and increased backing near the surface due to valley channeled flow (Lyza and Knupp 2018). To evaluate these hypotheses I conducted K-S tests and logistic regression analysis between tornadogenesis locations and spatially random points for the following variables: elevation, elevation slope and aspect, surface roughness, and slope and aspect of surface roughness. Two additional variables were also tested: population density, a known human-induced bias in the dataset (Anderson et al. 2007), and road proximity, a metric representing the accessibility of damage locations to surveyors. Road distance was by far the most strongly correlated variable with the location of tornadogenesis (KS score = 0.41221234), followed by surface roughness (0.26738944), population density (0.19402652), and elevation (0.14075218). Visual examination of the CDFs for each variable reveals that the trend is for higher elevations, medium-high population densities, lower surface roughness, and lower road distance. In the multivariate logistic regression, the results were much the same with the exception that surface roughness dropped out as a statistically significant factor, suggesting that its significance in the univariate analysis was an artifact of codependence with another factor. The strength of association with road proximity suggests that accessibility to damaged areas is a key driver in the recorded locations of tornadogenesis.

Given the importance of a robust tornado climatology for understanding public risk perception (Johnson et al. 2021), improving forecasts and dynamic understanding (e.g., Kellner and Niyogi 2014; Hua and Chavas 2019), and public safety and infrastructure planning (Ramsdell et al. 2007), it is valuable to explore additional tools to augment the existing ground survey methods. The tasseled cap derived disturbance index is useful for this purpose because it is able to provide useful information beyond simple visual inspection from single post storm images. Recently, tasseled cap transforms for Sentinel-2 were published (Shi and Xu 2019), enabling this approach to be used with higher resolution imagery that the previous Landsat derived applications (Kingfield and de Beurs 2017). I selected fourteen scenes totaling 50 tornados to analyze covering a variety of strengths, widths, seasonalities, land cover classes, and geographic locations. The DI were summarized by general land cover type and damage intensity rating. Using a Spearman ranked correlation coefficient, the DI was shown to be positively correlated with EF damage intensity for all landcover types.

The predictive skill of the DI was assessed by calculating the area under the receiver operator characteristic curve (AUROC) for each combination of landcover type and damage intensity. The largest increase in predictive skill was between EF1 and EF2 for all land cover types, suggesting a lower threshold for detectability somewhere in the upper end of EF1 to lower end of EF2 damage. This is similar to the value reported in other studies using coarser resolution satellites (Jedlovec et al. 2006; Molthan et al. 2014). The ability of the disturbance index to characterize tornadic damage was also highly dependent on the land cover type, performing best in the forested areas that it was designed for and most poorly in barren, developed, shrubby, grassy, or cultivated areas. This is also true of other studies that have used DI (Kingfield and de Beurs 2017) and those that have used other vegetation based spectral indices (Jedlovec et al.

2006; Molthan et al. 2014). There is also large uncertainty due to high levels of intra-class variation, especially with regard to tree cover in urban or barren areas. While the increased spatial resolution does not appear to lower the minimum damage threshold for detectability, it does yield a more spatially detailed picture of the damage field, which is useful for understanding tornadic behavior.

It is clear that remote sensing will have to play a role in further improving tornado surveys. While survey personnel will remain crucial to the process for the foreseeable future, our results demonstrate that satellite remote sensing can be a useful tool for filling in the blind spots of traditional survey methods. The techniques demonstrated here take advantage of relatively high temporal resolution data and perform best in areas where traditional ground-based surveys are most difficult such as forests and wetlands. The utility of satellite remote sensing can be further enhanced by the incorporation of more sophisticated object detection and additional spectral indices tailored to the underlying landcover type. Additional streamlining in the form of tasked, high-resolution imagery and targeted analysis based on radar velocity signatures could further optimize the process. As the process of identifying damage swaths in imagery becomes more refined, retrospective analysis on older data could also be used to augment traditional surveys for previous events where surveyors may not have had the opportunity to investigate all of the potential tracks. The operationalizing of these techniques will improve our understanding of tornadic processes with the goal of improving forecasting ability.

References

Agee, E., and S. Childs, 2014: Adjustments in Tornado Counts, F-Scale Intensity, and Path Width for Assessing Significant Tornado Destruction. *Journal of Applied Meteorology and Climatology*, **53**, 1494–1505.

Anderson, C. J., C. K. Wikle, Q. Zhou, and J. A. Royle, 2007: Population Influences on Tornado Reports in the United States. *Weather and Forecasting*, **22**, 571–579, https://doi.org/10.1175/WAF997.1.

Bell, J. M., Andrew L. ;. Schultz, Lori A., 2019: The 3 March 2019 Tornado Outbreak: A look from space.

de Beurs, K. M., B. C. Owsley, and J. P. Julian, 2016: Disturbance analyses of forests and grasslands with MODIS and Landsat in New Zealand. *International Journal of Applied Earth Observation and Geoinformation*, **45**, 42–54, https://doi.org/10.1016/j.jag.2015.10.009.

Bluestein, H. B., 2000: A Tornadic Supercell over Elevated, Complex Terrain: The Divide, Colorado, Storm of 12 July 1996. *Monthly Weather Review*, **128**, 795–809, https://doi.org/10.1175/1520-0493(2000)128<0795:ATSOEC>2.0.CO;2.

Bosart, L. F., A. Seimon, K. D. LaPenta, and M. J. Dickinson, 2006: Supercell Tornadogenesis over Complex Terrain: The Great Barrington, Massachusetts, Tornado on 29 May 1995. *Weather and Forecasting*, **21**, 897–922, https://doi.org/10.1175/WAF957.1.

Brooks, H. E., C. A. Doswell, and M. P. Kay, 2003: Climatological Estimates of Local Daily Tornado Probability for the United States. *Weather and Forecasting*, **18**, 626–640, https://doi.org/10.1175/1520-0434(2003)018<0626:CEOLDT>2.0.CO;2.

Claverie, M., J. G. Masek, J. Ju, and J. L. Dungan, 2017: Harmonized landsat-8 sentinel-2 (HLS) product user's guide.

Crist, E. P., 1984: Application of the Tasseled Cap Concept to Simulated Thematic Mapper Data. *Photogrammetric Engineering*,.

DaSilva, M. D., D. Bruce, P. A. Hesp, and G. Miot da Silva, 2021: A New Application of the Disturbance Index for Fire Severity in Coastal Dunes. *Remote Sensing*, **13**, 4739, https://doi.org/10.3390/rs13234739.

Dessens, J., Jr., 1972: Influence of Ground Roughness on Tornadoes: A Laboratory Simulation. *Journal of Applied Meteorology*, **11**, 72–75, https://doi.org/10.1175/1520-0450(1972)011<0072:IOGROT>2.0.CO;2.

Dixon, P. G., A. E. Mercer, J. Choi, and J. S. Allen, 2011: Tornado Risk Analysis: Is Dixie Alley an Extension of Tornado Alley? *Bulletin of the American Meteorological Society*, **92**, 433–441, https://doi.org/10.1175/2010BAMS3102.1.

Doswell, C. A., and D. W. Burgess, 1988: On Some Issues of United States Tornado Climatology. *Monthly Weather Review*, **116**, 495–501, https://doi.org/10.1175/1520-0493(1988)116<0495:OSIOUS>2.0.CO;2.

——, H. E. Brooks, and N. Dotzek, 2009: On the implementation of the enhanced Fujita scale in the USA. *Atmospheric Research*, **93**, 554–563, https://doi.org/10.1016/j.atmosres.2008.11.003.

Dwomoh, F. K., and M. C. Wimberly, 2017: Fire regimes and forest resilience: alternative vegetation states in the West African tropics. *Landscape Ecol*, **32**, 1849–1865, https://doi.org/10.1007/s10980-017-0553-4.

Edwards, R., H. E. Brooks, and H. Cohn, 2021: Changes in Tornado Climatology Accompanying the Enhanced Fujita Scale. *Journal of Applied Meteorology and Climatology*, https://doi.org/10.1175/JAMC-D-21-0058.1.

Finley, J. P., 1884: Character of six hundred tornadoes. *US Signal Service Professional Paper*, **7**, 16.

Frazier, A. E., B. L. Hemingway, and J. P. Brasher, 2019: Land surface heterogeneity and tornado occurrence: an analysis of Tornado Alley and Dixie Alley. *Geomatics, Natural Hazards and Risk*, **10**, 1475–1492, https://doi.org/10.1080/19475705.2019.1583292.

Gorelick, N., M. Hancher, M. Dixon, S. Ilyushchenko, D. Thau, and R. Moore, 2017: Google Earth Engine: Planetary-scale geospatial analysis for everyone. *Remote Sensing of Environment*, https://doi.org/10.1016/j.rse.2017.06.031.

Healey, S. P., W. B. Cohen, Y. Zhiqiang, and O. N. Krankina, 2005: Comparison of Tasseled Cap-based Landsat data structures for use in forest disturbance detection. *Remote Sensing of Environment*, **97**, 301–310, https://doi.org/10.1016/j.rse.2005.05.009.

Hirth, B. D., J. L. Schroeder, C. C. Weiss, D. A. Smith, and M. I. Biggerstaff, 2012: Research Radar Analyses of the Internal Boundary Layer over Cape Canaveral, Florida, during the Landfall of Hurricane Frances (2004). *Weather and Forecasting*, **27**, 1349–1372, https://doi.org/10.1175/WAF-D-12-00014.1.

Hodges, J. L., 1958: The significance probability of the smirnov two-sample test. *Arkiv för Matematik*, **3**, 469–486, 18.

Homer, C., and J. Dewitz, 2018: NLCD 2016. https://doi.org/10.5066/P937PN4Z.

Houser, J. B., N. McGinnis, K. M. Butler, H. B. Bluestein, J. C. Snyder, and M. M. French, 2020: Statistical and Empirical Relationships between Tornado Intensity and Both Topography and Land Cover Using Rapid-Scan Radar Observations and a GIS. *Monthly Weather Review*, **148**, 4313–4338, https://doi.org/10.1175/MWR-D-19-0407.1.

Hua, Z., and D. R. Chavas, 2019: The Empirical Dependence of Tornadogenesis on Elevation Roughness: Historical Record Analysis Using Bayes's Law in Arkansas. *Journal of*

Applied Meteorology and Climatology, **58**, 401–411, https://doi.org/10.1175/JAMC-D-18-0224.1.

Jedlovec, G. J., U. Nair, and S. L. Haines, 2006: Detection of Storm Damage Tracks with EOS Data. *Weather and Forecasting*, **21**, 249–267, https://doi.org/10.1175/WAF923.1.

Johnson, V. A., K. E. Klockow-McClain, R. A. Peppler, and A. M. Person, 2021: Tornado Climatology and Risk Perception in Central Oklahoma. *Weather, Climate, and Society*, **13**, 743–751, https://doi.org/10.1175/WCAS-D-20-0137.1.

Karstens, C. D., W. A. Gallus, B. D. Lee, and C. A. Finley, 2013: Analysis of Tornado-Induced Tree Fall Using Aerial Photography from the Joplin, Missouri, and Tuscaloosa–Birmingham, Alabama, Tornadoes of 2011. *Journal of Applied Meteorology and Climatology*, **52**, 1049–1068, https://doi.org/10.1175/JAMC-D-12-0206.1.

Kellner, O., and D. Niyogi, 2014: Land Surface Heterogeneity Signature in Tornado Climatology? An Illustrative Analysis over Indiana, 1950–2012*. *Earth Interactions*, **18**, 1–32, https://doi.org/10.1175/2013EI000548.1.

Kingfield, D. M., and K. M. de Beurs, 2017: Landsat Identification of Tornado Damage by Land Cover and an Evaluation of Damage Recovery in Forests. *Journal of Applied Meteorology and Climatology*, **56**, 965–987, https://doi.org/10.1175/JAMC-D-16-0228.1.

Lewellen, D. C., 2012: Effects of Topography on Tornado Dynamics: A Simulation Study. 26th Conference on Severe Local Storms (5 - 8 November 2012), AMS https://ams.confex.com/ams/26SLS/webprogram/Paper211460.html (Accessed July 1, 2023).

Lyza, A. W., and K. R. Knupp, 2018: A Background Investigation of Tornado Activity across the Southern Cumberland Plateau Terrain System of Northeastern Alabama. *Monthly Weather Review*, **146**, 4261–4278, https://doi.org/10.1175/MWR-D-18-0300.1.

——, T. A. Murphy, B. T. Goudeau, P. T. Pangle, K. R. Knupp, and R. A. Wade, 2020: Observed Near-Storm Environment Variations across the Southern Cumberland Plateau System in Northeastern Alabama. *Monthly Weather Review*, **148**, 1465–1482, https://doi.org/10.1175/MWR-D-19-0190.1.

Markowski, P. M., and N. Dotzek, 2011: A numerical study of the effects of orography on supercells. *Atmospheric Research*, **100**, 457–478, https://doi.org/10.1016/j.atmosres.2010.12.027.

McDonald, J. R., and K. C. Mehta, 2006: A Recommendation for an ENHANCED FUJITA SCALE (EF-Scale).

Molthan, A., J. Bell, T. Cole, and J. Burks, 2014: Satellite-based identification of tornado damage tracks from the 27 April 2011 severe weather outbreak. *J. Operational Meteor.*, **2**, 191–208, https://doi.org/10.15191/nwajom.2014.0216.

Muncy, T. J., 2021: Topographic and Surface Roughness Influences on Tornadogenesis and Decay. Ohio University, https://etd.ohiolink.edu/apexprod/rws_olink/r/1501/10?clear=10&p10_accession_num=ohiou1628513174226383 (Accessed July 1, 2023).

NOAA, *Frequent Questions: Coastal Change Analysis Program (C-CAP) Regional Land Cover*. National Oceanic and Atmospheric Administration,.

——, Damage Assessment Toolkit. https://apps.dat.noaa.gov/stormdamage/damageviewer/ (Accessed December 7, 2022b).

NSSL, PERiLS: Propagation, Evolution, and Rotation in Linear Storms. *NOAA National Severe Storms Laboratory*,. https://www.nssl.noaa.gov/projects/perils/ (Accessed March 22, 2024).

Ramsdell, J., J. Rishel, and A. Buslik, 2007: *Tornado climatology of the contiguous United States. Nuclear Regulatory Commission Rep*. Pacific Northwest National Laboratory,.

Schneider, D., 2009: The Impact of Terrain on Three Cases of Tornadogenesis in the Great Tennessee Valley. *Electronic Journal of Operational Meteorology*, **10**, 1–33.

Shi, T., and H. Xu, 2019: Derivation of Tasseled Cap Transformation Coefficients for Sentinel-2 MSI At-Sensor Reflectance Data. *IEEE Journal of Selected Topics in Applied Earth Observations and Remote Sensing*, **12**, 4038–4048, https://doi.org/10.1109/JSTARS.2019.2938388.

Shikhov, A., and A. Chernokulsky, 2018: A satellite-derived climatology of unreported tornadoes in forested regions of northeast Europe. *Remote Sensing of Environment*, **204**, 553–567, https://doi.org/10.1016/j.rse.2017.10.002.

Singh, A., 1989: Review Article Digital change detection techniques using remotely-sensed data. *International Journal of Remote Sensing*, **10**, 989–1003, https://doi.org/10.1080/01431168908903939.

SPC, 2018: Severe Weather Database.

Speheger, D. A., C. A. Doswell, and G. J. Stumpf, 2002: The Tornadoes of 3 May 1999: Event Verification in Central Oklahoma and Related Issues. *Weather and Forecasting*, **17**, 362–381, https://doi.org/10.1175/1520-0434(2002)017<0362:TTOMEV>2.0.CO;2.

USGS, National Elevation Dataset.

Verbout, S. M., H. E. Brooks, L. M. Leslie, and D. M. Schultz, 2006: Evolution of the U.S. Tornado Database: 1954–2003. *Weather and Forecasting*, **21**, 86–93, https://doi.org/10.1175/WAF910.1.

Wagner, M. A., S. W. Myint, and Randall. S. Cerveny, 2012: Geospatial Assessment of Recovery Rates Following a Tornado Disaster. *IEEE Transactions on Geoscience and Remote Sensing*, **50**, 4313–4322, https://doi.org/10.1109/TGRS.2012.2191973.

——, R. K. Doe, A. Johnson, Z. Chen, J. Das, and R. S. Cerveny, 2019: Unpiloted Aerial Systems (UASs) Application for Tornado Damage Surveys: Benefits and Procedures. *Bulletin of the American Meteorological Society*, **100**, 2405–2409, https://doi.org/10.1175/BAMS-D-19-0124.1.

Walsh, E., and S. Tezak, 2013: Findings and Recommendations of FEMA's Mitigation Assessment Team Investigations of the Spring 2011 Tornado Outbreaks. 821–830, https://doi.org/10.1061/9780784412640.087.

Wang, J., S. Cao, W. Pang, and J. Cao, 2017: Experimental Study on Effects of Ground Roughness on Flow Characteristics of Tornado-Like Vortices. *Boundary-Layer Meteorol*, **162**, 319–339, https://doi.org/10.1007/s10546-016-0201-6.

Witt, A., M. D. Eilts, G. J. Stumpf, E. D. W. Mitchell, J. T. Johnson, and K. W. Thomas, 1998: Evaluating the Performance of WSR-88D Severe Storm Detection Algorithms. *Weather and Forecasting*, **13**, 513–518, https://doi.org/10.1175/1520-0434(1998)013<0513:ETPOWS>2.0.CO;2.

Yang, L., and Coauthors, 2018: A new generation of the United States National Land Cover Database: Requirements, research priorities, design, and implementation strategies. *ISPRS Journal of Photogrammetry and Remote Sensing*, **146**, 108–123, https://doi.org/10.1016/j.isprsjprs.2018.09.006.